Cardiovascular Engineering and Technology, Vol. 13, No. 3, June 2022 *(© 2021)* pp. 504–513
https://doi.org/10.1007/s13239-021-00590-3

Short Communication

Spectral-Clustering of Lagrangian Trajectory Graphs: Application to Abdominal Aortic Aneurysms

AHMED DARWISH [1,2] SHAHRZAD NOROUZI [1] and LYES KADEM [1]

[1]Laboratory of Cardiovascular Fluid Dynamics, Concordia University, Montréal, QC H3G 1M8, Canada; and [2]Mechanical Engineering Department, Assiut University, 71515 Assiut, Egypt

(Received 9 June 2021; accepted 1 November 2021; published online 29 November 2021)

Associate Editor Igor Efimov oversaw the review of this article.

Abstract
Purpose—Identification of coherent structures in cardiovascular flows is crucial to describe the transport and mixing of blood. Coherent structures can highlight locations where minimal blood mixing takes place, thus, potential thrombus formation can be expected thither. Graph-based approaches have recently been introduced in order to describe fluid transport and mixing between multiple Lagrangian trajectories, where each trajectory serves as a node that can be connected to another trajectory based on their relative distance during the course of time. *Methods*—In this study, we compute the Lagrangian trajectories from *in vitro* planar instantaneous velocity fields in two models of abdominal aortic aneurysms, (AAA) namely single bulge and bi-lobed. Then, we construct unweighted and undirected graphs based on the pairwise distance of Lagrangian trajectories. We report local measures of the graph namely the degree and the clustering coefficient. We also perform spectral clustering of the graph Laplacian to extract the flow coherent sets. *Results*—Local graph measures reveal fluid regions of high mixing such as vortex boundaries. Through spectral clustering, the fluid is partitioned into a reduced number of coherent sets where within each set, inner mixing of fluid is maximized while the fluid mixing between different coherent sets is minimized. The approach reveals multiple coherent sets adjacent to the AAA bulge that have sustained this adjacency to the wall through their coherent motion during one cardiac cycle.
Conclusion—Identifying coherent sets enables tracking their transport during the cardiac cycle and identify their role in the flow dynamics. Moreover, the size and the transport of the long residing coherent sets inside the AAA bulges can be deduced which may aid in predicting thrombus formation at such location.

Keywords—Lagrangian trajectories graph, Spectral clustering, Abdominal aortic aneurysms, Flow coherent sets.

INTRODUCTION

In time dependent flows, we can identify coherent structures by adding passive particles to the flow. Such coherent structures organize the particles in recognizable patterns or regions–that last for a relatively long times—where fluid transport and mixing can be promoted or inhibited.[6] Identifying the Lagrangian coherent structures (LCS) in blood flow gained major attention as their identification can reveal flow recirculation or separation and characterize mixing in cardiovascular systems.[4,10,11,16,23] Four major Lagrangian approaches have been used to identify coherent structures in various fluid flows, namely geometric, probabilistic, braid-based and trajectory-based graph, see Ref. 1 and 5 for comprehensive reviews of these approaches.

In geometric approaches, obtaining eigenvectors and eigenvalues of the right Cauchy–Green strain tensor is the pivotal analysis. Such task requires the knowledge of highly resolved spatial derivatives of a given flow map. Then, the identified repelling and attracting material surfaces and lines can be visualized by plotting the finite-time Lyapunov exponent (FTLE) fields. Among the four approaches, the geometric approach has been extensively used in cardiovascular

Address correspondence to Ahmed Darwish, Laboratory of Cardiovascular Fluid Dynamics, Concordia University, Montréal, QC H3G 1M8, Canada. Electronic mail: lcfd@encs.concordia.ca, ahmeddiaa@aun.edu.eg

Ahmed Darwish and Shahrzad Norouzi contributed equally to this work.

flows to deduce LCS. For instance, higher potential of platelet activation (due to elevated level of accumulated shear stresses) is reported to be maximized along repelling LCS in a stenotic vessel[24] or downstream of a dysfunctional bileaflet mechanical aortic valve.[10] Furthermore, as the left ventricle (LV) can be a potential location for mural thrombus formation in patients with myocardial infarction, Badas *et al.*[4] used FTLE fields to identify critical flow structures that do not reach the LV apex. The AAA is another potential location for mural and intra-luminal thrombus. Arzani and Shadden[3] used, therefore, FTLE fields to show that LCS reveal—precisely—the location of flow separation, vortex transport, fluid mixing regions and flow impingement. Revealing the fluid transport skeleton, in an AAA, can aid educing the mechanism of thrombus formation and AAA progression.[3] This follows the finding of Bluestein *et al.*[8] and Biasetti *et al.*[7] who noticed that platelet activation and deposition on the AAA wall is correlated to blood recirculation and stasis inside the AAA bulge. Shadden and Arzani[23] provide a thorough review of geometric techniques to identify Lagrangian coherent structures in cardiovascular flows.

The probabilistic approach is centered around the discrete version of the Perron-Frobenius operator which requires, first, discretization of the fluid domain into a number of boxes (each box represents a node). By seeding each box with a defined number of Lagrangian particles at an initial advection time, the transfer operator is estimated from the flow among each pair of boxes after a defined time interval. Consequently, from a graph theoretic point of view, a weighted-directed graph can be constructed between the boxes spanning the flow domain resulting in a complex network. By using basic graph measures such as the in- and out-degree, one can deduce information about the fluid mixing, backward stretching, forward fluid stretching and fluid dispersion.[22] Similar to the geometric approach, the probabilistic approach also requires dense and highly resolved Lagrangian trajectories, thus both methods are computationally expensive.

In braids approach, the two dimensional physical space of a sparse set of trajectories is used as a base to include the time, thus forming a three dimensional space. By projecting the trajectories on one of the physical axes, we can detect a fluid coherent region by finding the individual trajectories that form a braid (similar to a rope), such region is called a coherent bundle.[2] Recently, Di Labbio *et al.*[12] applied braids approach to describe the intraventricular mixing and how the quality and complexity of mixing can be affected by different degrees of aortic regurgitation severity. Despite the ability of braids to handle sparse trajectories, advected particle positions are required to be known during the entire time interval. Moreover, due to its topological basis, braid theory can not be extended to three dimensional flows.[2]

The last approach, trajectory-based graph, used here, is computationally inexpensive and represents an objective method for identifying the coherent sets in cardiovascular flows. The central basis of this approach is a set of Lagrangian trajectories that can be sparse and incomplete.[6,14,15] As each trajectory acts as a node, a link is established between trajectories based on their Euclidean distance along the whole time interval as in Ref. 15. This method generates a weighted and undirected graph which can be computationally demanding. To further simplify the graph, Padberg-Gehle and Schneide[21] established a link between the trajectories that approach each other at least once during the given time interval. Therefore, the resulting graph becomes unweighted and undirected, significantly reducing the computational cost. Local measures of this simple graph such as the nodal degrees can reflect the amount of mixing each trajectory has with other trajectories. Additionally, the nodal clustering coefficient can indicate the trajectories that form a connected cluster (or subgraph) where all its neighbors become strongly connected. To extract the coherent sets, a spectral clustering approach is used with a k-means clustering algorithm to partition the graph into a defined number of coherent cluster sets. By doing so, one ensures that within each set, trajectories are highly connected while the connection between different set is minimized.

In this study, we will illustrate the application of the trajectory-based graph approach on *in vitro* planar instantaneous velocity fields in models of abdominal aortic aneurysms (AAA). Two geometries are investigated here, single bulge and bi-lobed AAAs. We will compute graph local measures (degree and clustering coefficient) and show their relation to mixing and blood transport. Moreover, we will highlight the transport of the coherent sets inside the two AAA models.

METHODS

Graph Construction from Lagrangian Flow Trajectories

For a given N Lagrangian particle trajectories in a time-dependent flow, a discrete-temporal representation of these trajectories during a defined time period $t \in [0, T]$ can be used as a starting point for the graph analysis, see (a) in Fig. 1. Each trajectory is considered as a node and all nodes are labeled as x_i with $i = 1,\ldots,$ N, and $x_{i,t} \in \mathbb{R}^2$. In cardiovascular flows, having direct

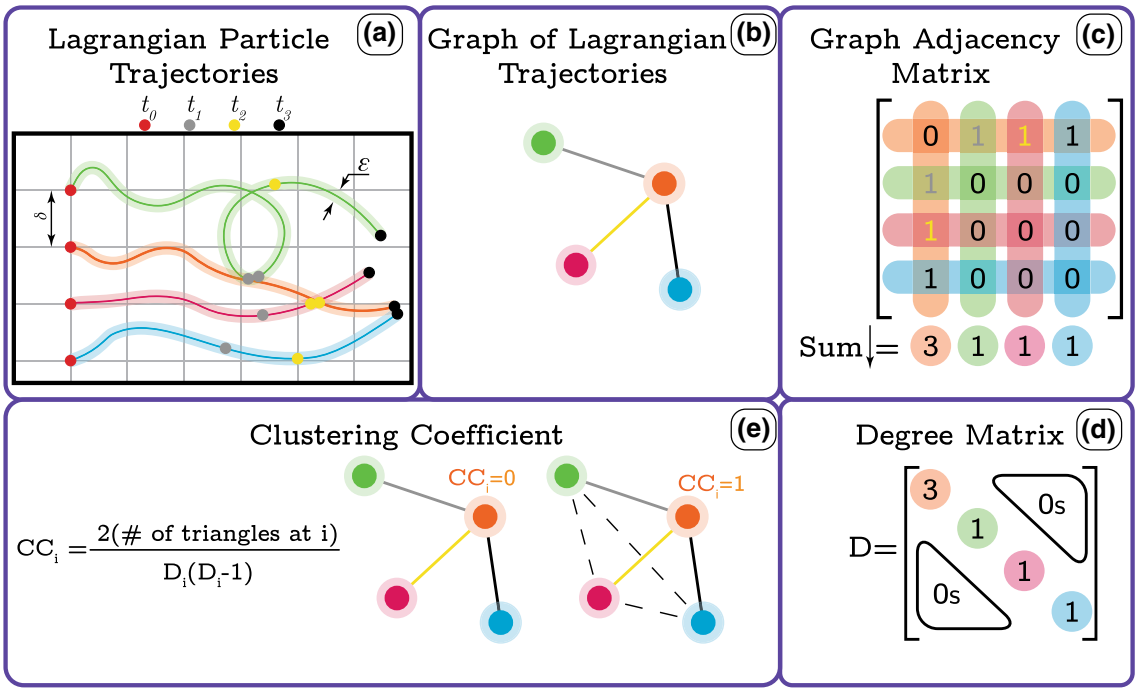

FIGURE 1. Graphical illustration of Lagrangian particle graph analysis. (a) Four Lagrangian trajectories originating from an initially located grid of particles being equally spaced with a distance δ. Each trajectory is given a different color with a faded region highlighting the ε search region along each trajectory. The Lagrangian particle location is highlighted by a circle which is colored based on the advection time (t_0—red, t_1—gray, t_2—yellow and t_3—black). (b) The graph constructed from the Lagrangian particle locations in (a). Each node represents a corresponding trajectory which becomes connected to another node, if they become ε-close to each other at any given time instant. The edges are colored based on the timing when the ε-closeness occurs between the trajectories. The adjacency matrix is shown in (c) which represents a pairwise connection matrix of the graph in (b). Each column and row is colored by its corresponding node (trajectory). Either a column-wise or a row-wise summation of the adjacency matrix gives the degree of each node. The degree matrix, in (d), holds the values of nodal-degree in its diagonal. (e) The computation of nodal clustering coefficients of the orange trajectory, CC_i, by using two graphs with different number of edges.

access to the Lagrangian trajectories can be challenging. In this cases, the first step is to define the initial time t_0 which corresponds to a velocity field $\mathbf{u}(\mathbf{x}, t_0)$ where a grid of Lagrangian particles will be located. The particles are uniformly spaced (in x–y directions) with a distance δ. Now, as the particles follow their Lagrangian trajectories in time for a time interval τ (using a fourth-order Runge–Kutta scheme), new positions will be reached at each intermediate time-step (between t_0 and $t_0 + \tau$) by each particle leading to a change in the distance between their respective trajectories. Then, an edge is added (to the network) if two trajectories come ε-close to each other at any time step during their temporal evolution, see (b) in Fig. 1. Later, a graphical representation of the network can be obtained, as in (b) of Fig. 1. However, the need to further analyse the network necessitates using a mathematical representation such as the adjacency matrix S19

$$\mathbf{S}_{ij} = \begin{cases} \underset{0\le t\le T}{max}\, 1_{\mathbb{C}_\varepsilon(x_{i,t})}(x_{j,t}), & i \neq j \\ 0, & i = j, \end{cases} \tag{1}$$

where $\mathbf{S}_{ij} = 1$, if an edge exists between two trajectories i and j. Under such condition, we can find the trajectory $x_{j,t}$ in a circle $\mathbb{C}_\varepsilon(x_{i,t})$, with ε-radius, away from $x_{i,t}$. Here, we need to select a value of $\varepsilon > 0$, a threshold that can be applied on the distance between the trajectories in the course of time interval τ. Notably, as the reported network is unweighted, we do not count the number of encounters between trajectories which means that trajectories that approach each other once have $S_{ij} = 1$ similar to that of trajectories that become closer more than once. Therefore, $\mathbf{S}$ is symmetric and represents an unweighted-undirected graph as shown in (c) of Fig. 1. To ensure that all nodes in the graph have at least one connection, the lower bound of ε should be selected based on the 2D Euclidean distance between the initially positioned particles. For instance, if the initial particle locations are distributed over an equally spaced grid, then ε must be more than or equal to the grid size spacing.

Nodal Degree

The local properties of the adjacency matrix can be easily mapped to each individual node; for instance the

nodal degree, D_i as in (2), is used to count the number of trajectories that become ε-close to a trajectory i. Then, the values of D_i form the diagonal matrix $\mathbf{D}$. Panels (c) and (d) in Fig. 1 graphically show the computation of the nodal degree matrix.

$$D_i = \sum_{j=1}^{N} S_{ij}, \quad i,j = 1,\ldots,N. \tag{2}$$

Clustering Coefficient

Another local graph property is the clustering coefficient which indicates the degree of inner connection between the neighbors of a certain node i, as in (3) (for undirected graphs)

$$CC_i = \frac{2(\#\ of\ triangles\ at\ node\ i)}{D_i(D_i-1)}. \tag{3}$$

So, for a given node i, a high clustering coefficient suggests that this node and its neighbors form a highly connected subgraph.

Threshold Selection

In general, the graph and its measures depend on the considered number of trajectories, the complexity of the flow and the initial condition of the trajectories.[13] However, the critical parameter for the graph analysis is ε.[13,21] Therefore, Donner *et al.*[13] linked the selection of ε to another graph parameter, the edge density $\rho(\varepsilon)$

$$\rho(\varepsilon) = \frac{2E(\varepsilon)}{N(N-1),} \tag{4}$$

where $E(\varepsilon)$ is the number of edges in the adjacency matrix for a selected ε. As the reader can notice, for a given number of trajectories N, increasing ε will increase the edge density, thus the adjacency matrix will become dense and more expensive –computationally– to handle. By selecting large ε values, the coherent sets identified by graph measures become less representative of the flow dynamics as reported in Ref. 21. Therefore, following the suggestion of Donner *et al.*,[13] we select a value for ε to lead to $\rho(\varepsilon) \leq 0.05$.

Spectral Graph Partitioning

Graph partitioning aims to dividing the graph into a set of subgraphs where nodes in each subgraph are strongly connected while all subgraphs are minimally connected amongst each.[19] To partition an unidirected graph, the Laplacian matrix is required. The graph Laplacian is another matrix that can describe a graph. For an unweighted and undirected graph, the Laplacian matrix is symmetric with its non-normalized form as defined in (5)

$$\mathbf{L} = \mathbf{D} - \mathbf{S}. \tag{5}$$

From the graph Laplacian and the degree matrix, Shi and Malik[25] proposed solving a normalized cut problem by considering the generalized eigenvalue problem in (6)

$$\mathbf{L}\boldsymbol{v} = \lambda\mathbf{D}\boldsymbol{v}. \tag{6}$$

Now, by sorting the eigenvalues in a ascending order as $0 = \lambda_1 \leq \lambda_2 \leq \cdots \leq \lambda_N$; the number of coherent sets (clusters) can be identified by finding the number of eigenvalues close to zero.[9] To heuristically accomplish such a task, we find the largest eigengap index k following Hadjighasem *et al.*[15] as in (7)

$$k = arg\,min_i[\max(\lambda_{i+1} - \lambda_i)]. \tag{7}$$

To extract the desired k clusters, we apply the standard k-means clustering algorithm[17] using the eigenvectors $\boldsymbol{v_i}$, with $i = 1,2,\ldots,k$. In k-mean clustering algorithm, k number of centers are created within $\mathbb{R}^2$ with a task to minimize the mean-square distance between each node and its closest center, thus each node can be assigned to a center (a cluster). By doing so, we ensure that all trajectories within a cluster have strong connections between each other and weak connections with the remaining trajectories.

Finally, in order to validate our algorithm, we use an analytical flow called the Bickleyjet. The identified coherent sets match the ones reported in Ref. 21. The reader is referred to Appendix—Supplementary Materials for more details.

APPLICATIONS

Abdominal Aortic Aneurysms

To cluster the trajectories in AAA flows, we report the flow inside two models of AAA namely single bulge and a bi-lobed AAAs, see Ref. 20 for more details. By using an *in vitro* setup as shown in Fig. 2, the flow fields are measured using time-resolved planar particle image velocimetry technique. The inlet flow waveforms for both cases are shown in Fig. 2. These waveforms correspond to a heart rate of 63 bpm while the Womersely number at the AAA inlet is 13.2. The resulting mean Reynolds number for all cases is 344 ± 7. As the duration of one cardiac cycle T is 0.953 s, the time axis in Fig. 2 is normalized so that it indicates $t^* = t/T$. The original instantaneous 2D flow fields are resolved over a grid with 0.6 mm spacing in both x and y directions and a temporal resolution of

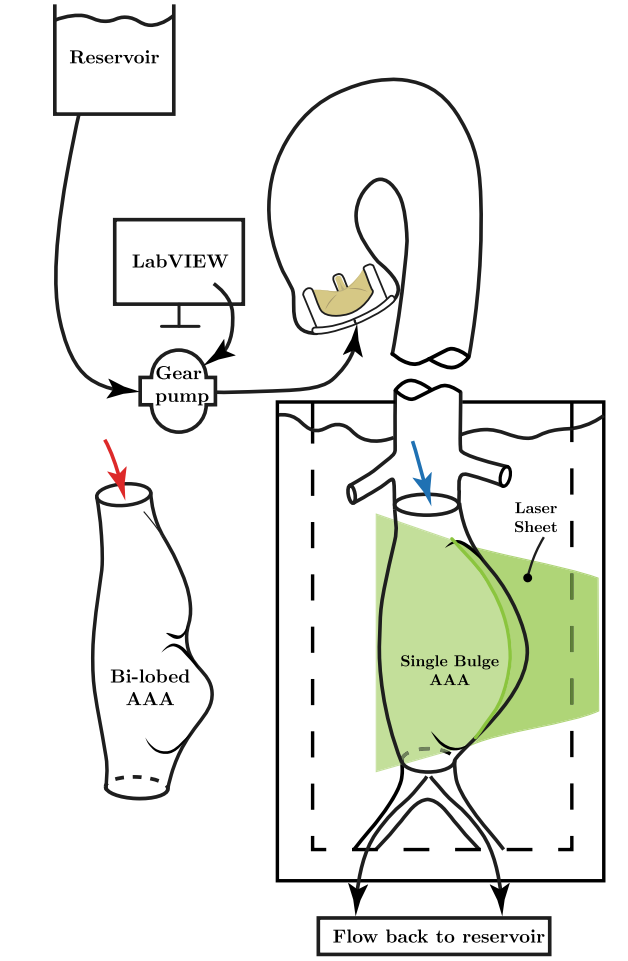

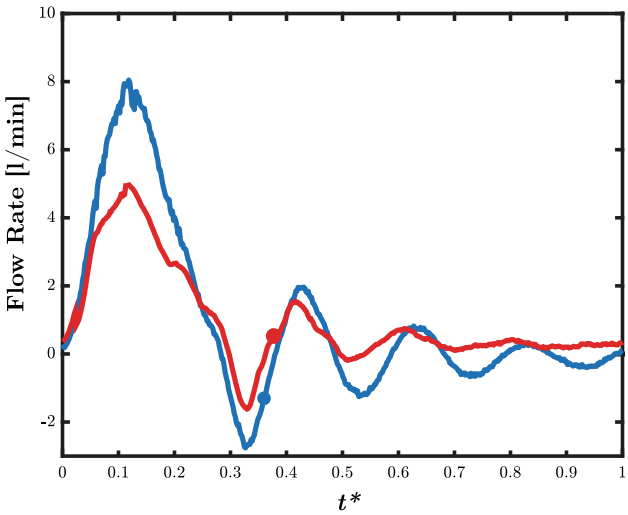

◀FIGURE 2. The top part shows a schematic of the experimental setup where the aortic model includes the ascending aorta, the aortic arch, the descending aorta, and the infrarenal abdominal aorta. At the infrarenal abdominal aortic section, AAA model can be placed. The reported two AAA models (single bulge and bi-lobed) are shown. Each AAA model ends with aortic bifurcation into the left and right common iliac arteries. The flow is produced by the means of a gear pump with its motor being controlled *via* LabVIEW interface. The outlet of the pump is connected to the aortic inlet where a bioprosthetic valve is placed. The pump received the working fluid from a high reservoir to ensure a physiological mean aortic pressure. To close the circuit, the flow passes from the iliac arteries back into the reservoir. The bottom part shows the inlet flow waveform to the bi-lobed AAA (in red) and the single bulge AAA (in blue) are shown. The initial release time of the Lagrangian particles (t_0) is highlighted with a small circle on each flow rate curve.

1.9×10^{-3} s. Table 1 summarizes the experimental conditions that have been used to acquire the velocity fields in both AAA models.

Initially, particles on a uniform grid (spaced at δ = 1 mm) are released shortly after systole at a selected t_0 as shown in Fig. 2. A bi-cubic interpolation is performed to acquire the velocities at non original locations. Then, as particles are treated as passive, they are advected in time using a fourth-order Runge–Kutta scheme to find their locations at each intermediate time-step between t_0 and $t_0 + \tau$ with $\tau = 1$. The new particle location is extracted at each time instant of the original velocity fields. For graph construction, we select $\varepsilon = 2\delta$ (double the value of the initial particle spacing) to ensure graph connectivity. Thus, every node in the graph has to be connected, at least, to another node. The values of edge density $\rho(\varepsilon)$ are 0.0178 and 0.021 for the single bulge and the bi-lobed AAAs, respectively.

For the single bulge AAA, nodal degrees and clustering coefficients show the initial location of the propagating vortex ring (see the instantaneous velocity field in Fig. 3). The vortex closer to the bulge has a relatively low degree and clustering coefficients. Notably, regions with high clustering coefficients will be mostly located at the vortex center, where the trajectories and their neighbours are strongly connected. For instance, the vortex closer to the bulge has relatively lower clustering coefficient value at its center when being compared with the other opposite vortex. This indicates that for the vortex closer to the bulge wall, trajectories are slightly distorted which justifies their relatively higher nodal degree. In the supplementary document, the reader can see the evolution of the trajectories which justifies their corresponding degree and clustering coefficient values. Now, between the vortex pair, a strip with high degree and low clustering coefficient can be noticed. As this high degree strip coincides with the core of the propagating jet, thus, a large number of trajectories are accelerated for a short period through the narrow jet core while being close to each other. Following this short acceleration, the trajectories start to diverge where they become ε-close to additional new trajectories. Clearly, as the nodal de-

TABLE 1. Summary of the experimental conditions.

Working fluid properties	Water–glycerol ratio	60–40 (% by volume)
	Density (ρ)	1160 kg/m^3
	Dynamic viscosity (μ)	0.0041 Pa s
Simulator operating conditions	Infrarenal flow rate	1 ± 0.18 L/min
	Cardiac period	0.952 s
	Systolic pressure	153 ± 3 mmHg
	Diastolic pressure	± 3 mmHg
Recording resolution	Number of images/cardiac cycle	500
	Temporal resolution	1.9 ms
	Spatial resolution	0.6 mm

grees of these trajectories increase, their respective local clustering coefficients decrease due to the relatively weak connection between their new neighbours. To highlight this behavior of trajectories inside the jet core, further details have been included in the supplementary document. At the AAA inlet, a region with high degree and clustering coefficient can be observed; the opposite can be found at the AAA's outlet. Furthermore, the trajectories starting at the bulge have low degree and moderate clustering coefficient values. To identify the coherent sets, the spectral gap in the leading eigenvalues of the graph Laplacian identifies 15 clusters which are extracted by applying the k-means clustering algorithm. The clusters are shown in Fig. 4. To examine the temporal advection of the coherent sets, we show two time instants; one is after half a cardiac cycle has passed ($t_0 + 0.5$) and another after one complete cycle ($t_0 + 1$). For a more detailed view of the propagation of clusters, the reader can see the supplementary videos. The clusters closer to the AAA's outlet (4 faded clusters) have a relatively shorter life span as they leave the domain early, therefore they will be excluded from our discussion . Four clusters are adjacent to the bulge wall; these sets experienced minimal transport from their initial locations while keeping their attachment to the wall, as shown in Fig. 4. By advecting the clusters, we can notice that the initial boundary, of each cluster, deforms with the motion of the particles. However, the particles associated with each cluster keep a defined boundary that is minimally invaded by other clusters. For instance, see the blue cluster motion in Fig. 4 between ($t_0 + 0.5$) and ($t_0 + 1$). Interestingly, one cluster can identify the coherence of the posterior vortex between (t_0) and ($t_0 + 0.5$) in Fig. 4.

For the bi-lobed AAA, the narrower area of the aneurysm does not allow the development of a vortex ring. Under these conditions, the longitudinal region, facing the upper lobe, with high degree indicates higher mixing where trajectories mix with each other more frequently. Moreover, a low degree region can be noticed at the lower bulge and the posterior wall. The clustering algorithm identifies 9 coherent sets with the lower three sets leaving the domain first (being faded in Fig. 4). Three longitudinal coherent sets extend from the inlet where one is adjacent to the upper lobe, the second occupies the AAA center and extends to cover the junction between the two lobes and the third adjacent to the posterior wall. Another set includes the trajectories starting inside the lower lobe. These trajectories have minimally traveled away from their initial position, as shown in Fig. 4 and the supplementary video material.

DISCUSSION AND CONCLUSION

In this study, we apply the simplest and the most computationally-efficient trajectory-based approach to analyze the fluid transport within two AAA models. This approach uses an unweighted-undirected graph to describe the connectivity between a coarse grid of Lagrangian trajectories in the flow of interest. The graph is described by the adjacency matrix which is being sparse by connecting only the trajectories that become ε-close to each other at least once during their life span. By doing so, the graph considers the trajectories during all investigated time instants; unlike the case of probabilistic approach where the fluid transport is considered only at the initial and final time instants.[22] Using the simplest graph characteristics (i.e., node degree and clustering coefficients), we revealed regions with high or low mixing. Such characteristics are sensitive to the value of ε, therefore Donner *et al.*[13] suggested using an edge density $\rho(\varepsilon) \leq 0.05$ in order to identify more representative clusters of the dynamics in the investigated flow. Thus, we can construct a sparse adjacency matrix that can represent the investigated flow from a set of few trajectories. We also utilize the spectral analysis of the generalized graph Laplacian eigenvalue problem to extract the number of coherent sets in each investigated flow. The

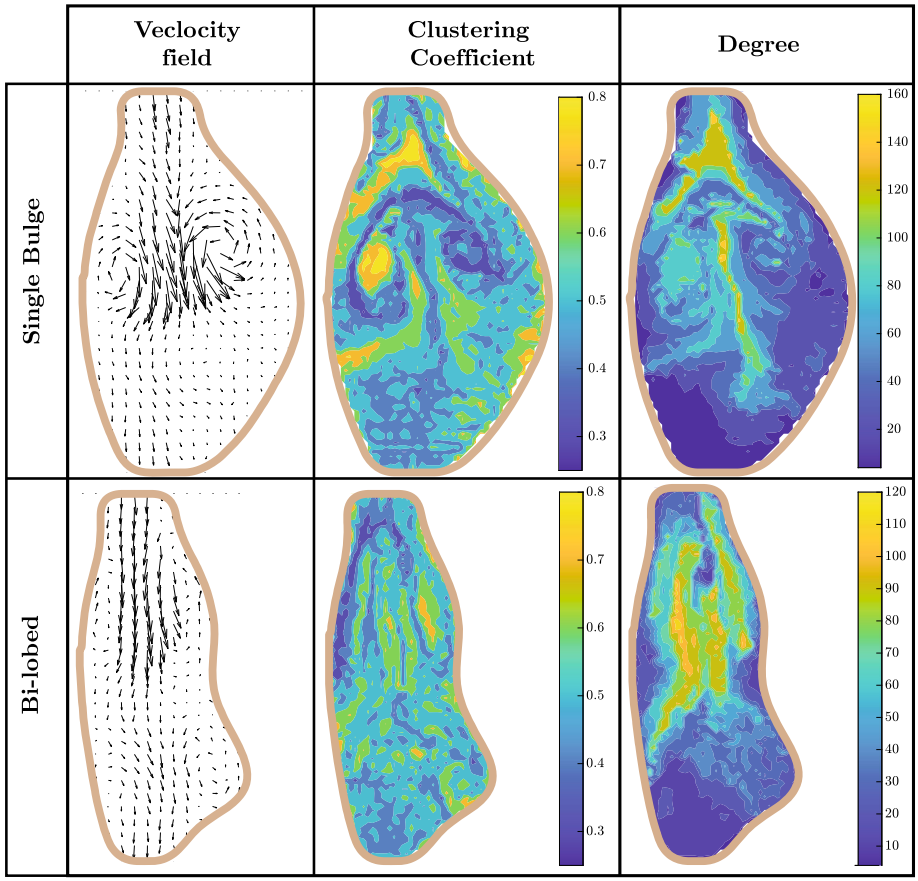

FIGURE 3. Left column shows the velocity fields in both AAA models at the initial particle advection time $t_0 = 0.402$ for the single bulge, and $t_0 = 0.39$ for the bi-lobed AAA. This time is indicated by a circle on each flow rate curves in Fig. 2. The middle and right columns show node degree and clustering coefficients for single bulge AAA (top row) and bi-lobed AAA (bottom row). The graph is evaluated for $\varepsilon = 2\delta$ and $\rho(\varepsilon) = 0.0178$ for the single bulge and $\rho(\varepsilon) = 0.021$ for the bi-lobed.

number of flow coherent sets (clusters) matches the index of the largest eigengap in the leading eigenvalues. The results show the ability of the clustering algorithm to define flow coherent sets where trajectories remain close under the considered time span.

In cardiovascular flows, revealing the coherent sets can help understanding the transport of individual sets (clusters), for instance, the clustering algorithm is able to identify the trajectories remaining inside the bulge in the case of an AAA. The distribution and size of these coherent sets can be related to the recirculation inside the aneurysm. For instance, Bluestein *et al.*[8] noticed that the flow recirculation region inside the aneurysm promotes thrombus formation and increases the possibility of rupture. A similar conclusion was drawn by Biasetti *et al.*[7] where they suggested that the platelet activation and deposition on the AAA wall can be attributed to the increased shear stress along the boundary of the long staying fluid inside the bulge. In this study, as the spectral clustering approach has been able to partition the fluid into different coherent clusters; by doing so, the approach has revealed the boundaries of these sets including the ones being adherent to the AAA wall.

Targeted drug delivery is another promising field where identification of flow coherent sets can be instrumental. Recently, Meschi *et al.*[18] reported that the LCS can be used to optimize an efficient targeted drug delivery. Furthermore, in liver cancer treatment, accurate and precise delivery of the radioactive dose—through the hepatic artery—only to the tumor ensures the efficacy of the treatment.[26] Notably, the flow coherent sets (*via* spectral clustering) show the origin of each set, while advecting the sets in time can show their destination. Therefore, they can provide a promising guiding map of potential initial injection locations that can maximize the likelihood to reaching the targeted destination.

Furthermore, the approach handles incomplete trajectories that flee the domain faster due to their closeness to the outlet; such ability was highlighted in Ref. 21. Additionally, the approach can be easily extended to three dimensional trajectories despite not being included in this study. Such approach can be

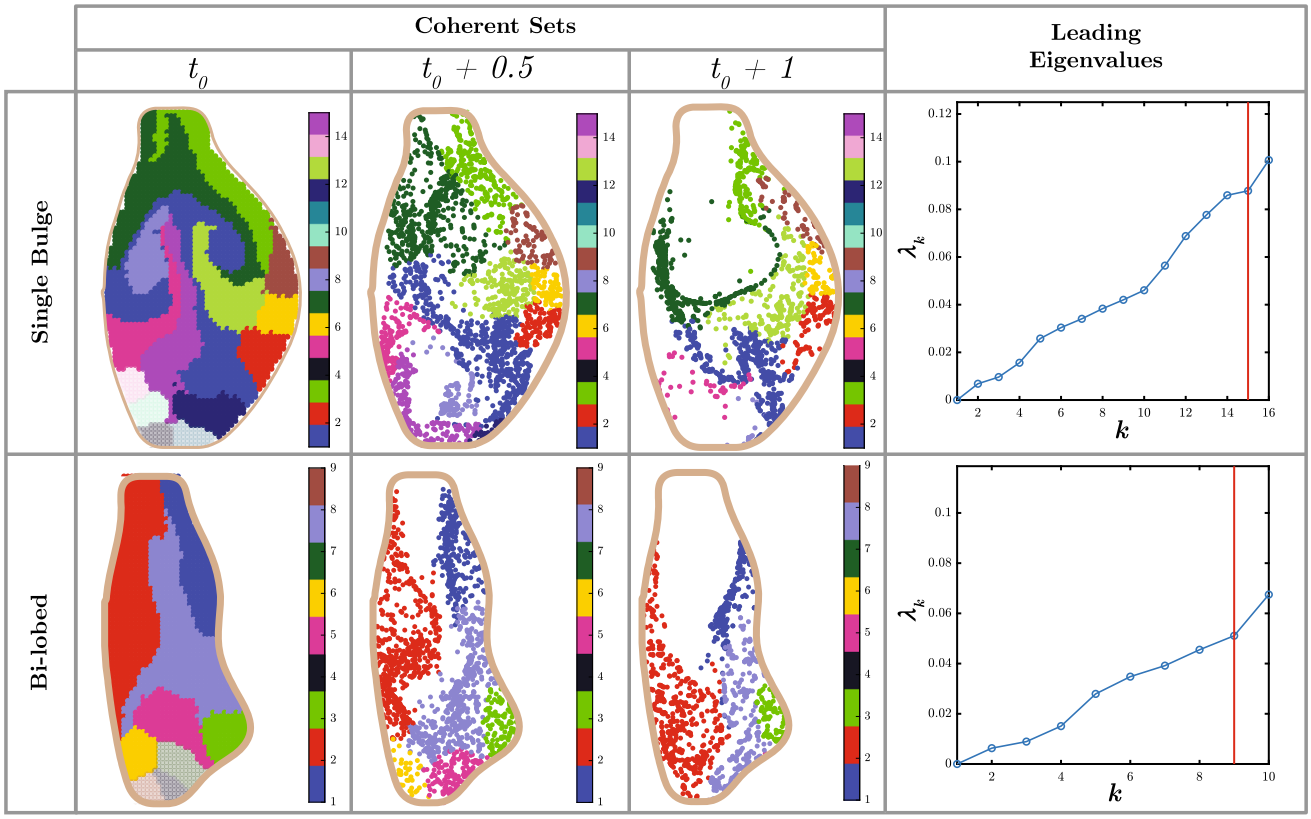

FIGURE 4. Identified coherent sets in single bulge and bi-lobed AAA at (t_0), ($t_0 + 0.5$) and ($t_0 + 1$). The initial particle advection time $t_0 = 0.402$ for the single bulge, and $t_0 = 0.39$ for the bi-lobed AAA. The right column shows the leading eigenvalues in each case with the eigengap being defined by the vertical red line. The graph is evaluated for $\varepsilon = 2\delta$ and $\rho(\varepsilon) = 0.0178$ for the single bulge AAA and $\rho(\varepsilon) = 0.021$ for the bi-lobed AAA.

directly implemented on three dimensional cardiovascular flows being acquired *via* 4D-MRI or ech-PIV. Under such condition, the trajectories can be connected if they become ε-close to each other, where ε will be the radius of a search sphere. Notably, the number of identified clusters depends on the initial release time, the value of ε and the edge density. For instance, to identify a coherent set that encompasses the intra-vortical structures, their presence in the flow field at the initial time is necessary.

The temporal resolution of the Lagrangian trajectories also affects the graph measures and the spectral clustering results, particularly in defining the vortical structures. Interestingly, the temporal resolution does not significantly affect the coherent sets adjacent to the AAA bulge. This can be attributed to the minimal transport of such coherent sets. Notably, the computational performance of the suggested algorithm can be ensured by using a relatively small number of trajectories. Clearly, using a small number of trajectories will reduce the size of the adjacency matrix $\mathbf{S}$, the graph Laplacian $\mathbf{L}$ and the degree matrix $\mathbf{D}$. Therefore, solving the normalized cut problem by considering the generalized eigenvalue problem in (6) will require less time and computational resources. Moreover, as the k-means clustering algorithm iteratively assigns each node (trajectory) to their nearest cluster, one can expect that for a larger number of nodes, higher computational resources could be required in order to obtain the coherent sets.

In conclusion, in this work, we have illustrated the applicability of spectral-clustering of particle trajectory graphs to cardiovascular flows and more specifically to the flow in models of AAAs. This is a very promising approach that identifies and tracks coherent sets in a flow field. This information is critical for the evaluation of the risks of sub-optimal mixing in the presence of cardiovascular disease or after the implantation of cardiovascular medical devices.

SUPPLEMENTARY INFORMATION

The online version contains supplementary material available at https://doi.org/10.1007/s13239-021-00590-3.

AUTHOR CONTRIBUTIONS

AD and LK conceptualized the study. SN designed and performed the experiments to provide the flow fields. AD developed the post-processing codes and performed the analysis. AD and LK wrote the original draft while all authors revised and edited the final manuscript. LK supervised the project and acquired the funding.

FUNDING

This work is supported by a grant from the Natural Sciences and Engineering Research Council of Canada (NSERC) (Grant No. 343164-07).

DATA AVAILABILITY

The codes used in this manuscript are available at https://github.com/AhmedDarwish466/TrajectoryBasedNetworks.

CONFLICT OF INTEREST

Ahmed Darwish, Shahrzad Norouzi and Lyes Kadem declare that they have no conflict ofinterest.

REFERENCES

[1]Allshouse, M. R., and T. Peacock. Lagrangian based methods for coherent structure detection. *Chaos* 25(9):097617, 2015. https://doi.org/10.1063/1.4922968.

[2]Allshouse, M. R., and J.-L. Thiffeault. Detecting coherent structures using braids. *Physica D* 241(2):95-105, 2012. https://doi.org/10.1016/j.physd.2011.10.002.

[3]Arzani, A., and S. C. Shadden. Characterization of the transport topology in patient-specific abdominal aortic aneurysm models. *Phys. Fluids* 24(8):081901, 2012. https://doi.org/10.1063/1.4744984.

[4]Badas, M. G., F. Domenichini, and G. Querzoli. Quantification of the blood mixing in the left ventricle using Finite Time Lyapunov Exponents. *Meccanica* 52(3):529–544, 2016. https://doi.org/10.1007/s11012-016-0364-8.

[5]Balasuriya, S., N. T. Ouellette, and I. I. Rypina. Generalized Lagrangian coherent structures. *Physica D* 372:31–51, 2018. https://doi.org/10.1016/j.physd.2018.01.011.

[6]Banisch, R., P. Koltai, and K. Padberg-Gehle. Network measures of mixing. *Chaos* 29(6):063125, 2019. https://doi.org/10.1063/1.5087632.

[7]Biasetti, J., F. Hussain, and T. C. Gasser. Blood flow and coherent vortices in the normal and aneurysmatic aortas: a fluid dynamical approach to intra-luminal thrombus formation. *J. R. Soc. Interface* 8(63):1449–1461, 2011. https://doi.org/10.1098/rsif.2011.0041.

[8]Bluestein, D., L. Niu, R. T. Schoephoerster, *et al*. Steady flow in an aneurysm model: correlation between fluid dynamics and blood platelet deposition. *J. Biomech. Eng.* 118(3):280-286, 1996. https://doi.org/10.1115/1.2796008.

[9]Chung, F. *Spectral Graph Theory*. Providence: American Mathematical Society, 1996. https://doi.org/10.1090/cbms/092.

[10]Darwish, A., G. Di Labbio, W. Saleh, *et al*. In vitro characterization of Lagrangian fluid transport downstream of a dysfunctional bileaflet mechanical aortic valve. *AIP Adv.* 10(9):095319, 2020. https://doi.org/10.1063/5.0021372.

[11]Di Labbio, G., J. Vétel, and L. Kadem. Material transport in the left ventricle with aortic valve regurgitation. *Phys. Rev. Fluids* 3(11):113101, 2018. https://doi.org/10.1103/physrevfluids.3.113101.

[12]Di Labbio, G., J.-L. Thiffeault, and L. Kadem. Deducing global mixing information in the heart from sparse particle trajectory data. APS Division of Fluid Dynamics Meeting Abstracts. APS Meeting Abstracts, January 2020.

[13]Donner, R. V., Y. Zou, J. F. Donges, *et al*. Ambiguities in recurrence-based complex network representations of time series. *Phys. Rev. E* 81(1):015101, 2010. https://doi.org/10.1103/physreve.81.015101.

[14]Froyland, G., and K. Padberg-Gehle. A rough-and-ready cluster-based approach for extracting finite-time coherent sets from sparse and incomplete trajectory data. *Chaos* 25(8):087406, 2015. https://doi.org/10.1063/1.4926372.

[15]Hadjighasem, A., D. Karrasch, H. Teramoto, *et al*. Spectral-clustering approach to Lagrangian vortex detection. *Phys. Rev. E* 93(6):063107, 2016. https://doi.org/10.1103/physreve.93.063107.

[16]Joly, F., G. Soulez, D. Garcia, *et al*. Flow stagnation volume and abdominal aortic aneurysm growth: insights from patient-specific computational flow dynamics of Lagrangian-coherent structures. *Comput. Biol. Med.* 92:98–109, 2018. https://doi.org/10.1016/j.compbiomed.2017.10.033.

[17]Lloyd, S. Least squares quantization in PCM. *IEEE Trans. Inf. Theory* 28(2):129-137, 1982. https://doi.org/10.1109/tit.1982.1056489.

[18]Meschi, S. S., A. Farghadan, and A. Arzani. Flow topology and targeted drug delivery in cardiovascular disease. *J. Biomech.* 119:110307, 2021. https://doi.org/10.1016/j.jbiomech.2021.110307.

[19]Newman, M. *Networks*. Oxford: Oxford University Press, 2010. https://doi.org/10.1093/acprof:oso/9780199206650.001.0001.

[20]Norouzi, S. Flow Characteristics in Abdominal Aortic Aneurysms: An in vitro Study. MA thesis. Concordia University, 2020.

[21]Padberg-Gehle, K., and C. Schneide. Network-based study of Lagrangian transport and mixing. *Nonlinear Processes Geophys.* 24(4):661–671, 2017. https://doi.org/10.5194/npg-24-661-2017.

[22]Ser-Giacomi, E., V. Rossi, C. López, *et al*. Flow networks: a characterization of geophysical fluid transport. *Chaos* 25(3):036404, 2015. https://doi.org/10.1063/1.4908231.

[23]Shadden, S. C., and A. Arzani. Lagrangian postprocessing of computational hemodynamics. *Ann. Biomed. Eng.* 43(1):41–58, 2014. https://doi.org/10.1007/s10439-014-1070-0.

[24]Shadden, S. C., and S. Hendabadi. Potential fluid mechanic pathways of platelet activation. *Biomech. Model. Mechanobiol.* 12(3):467–474, 2012. https://doi.org/10.1007/s10237-012-0417-4.

[25]Shi, J., and J. Malik. Normalized cuts and image segmentation. In Proceedings of IEEE Computer Society Conference on Computer Vision and Pattern Recognition. IEEE Computer Society. https://doi.org/10.1109/cvpr.1997.609407.

[26]Taebi, A., C. T. Vu, and E. Roncali. Multiscale computational fluid dynamics modeling for personalized liver cancer radioembolization dosimetry. *J. Biomech. Eng.* 143(1):011002, 2020. https://doi.org/10.1115/1.4047656.